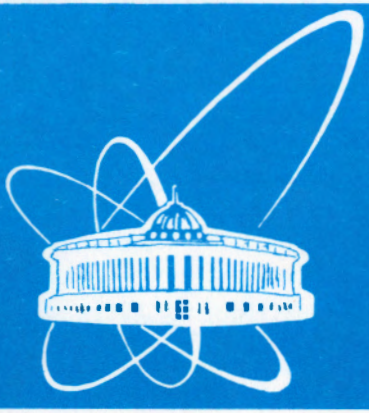

ОБЪЕДИНЕННЫЙ
ИНСТИТУТ
ЯДЕРНЫХ
ИССЛЕДОВАНИЙ

Дубна

00-152

E1-2000-152

Avdeyev S. P.

MULTIFRAGMENTATION OF GOLD NUCLEI BY LIGHT RELATIVISTIC IONS — THERMAL BREAK-UP VERSUS DYNAMIC DISINTEGRATION

Submitted to «Ядерная физика»

2000

S.P.Avdeyev, V.A.Karnaukhov, L.A.Petrov, V.K.Rodionov, V.D.Toneev
Joint Institute for Nuclear Research, 141980 Dubna, Russia

H.Oeschler
Institut für Kernphysik, Technische Universität Darmstadt, 64289 Darmstadt, Germany

O.V.Bochkarev, L.V.Chulkov, E.A.Kuzmin
Kurchatov Institute, 123182 Moscow, Russia

A.Budzanowski, W.Karcz, M.Janicki
H.Niewodniczanski Institute of Nuclear Physics, 31-342 Cracow, Poland

E.Norbeck
University of Iowa, Iowa City, IA 52242, USA

A.S.Botvina
INFN and Dipartimento di Fisica, 40126 Bologna, Italy

W.A.Friedman
Physics Department, University of Wisconsin, Madison, Wisconsin 53706, USA

K.K.Gudima
Institute of Applied Physics, Kishinev, Moldova

1 Introduction

Nuclear fragmentation was discovered in cosmic rays 60 years ago [1, 2] as a puzzling phenomenon in which nuclear fragments are emitted from collisions of relativistic protons with various targets. The observed fragments were heavier than α particles but lighter than fission fragments. Now, they are commonly called Intermediate Mass Fragments (IMF, $3 \leq Z \leq 20$). Later on, in the fifties, this phenomenon was first observed in accelerator experiments [3] and then studied leisurely for three decades. The situation has been changed dramatically after 1982 when multiple emission of IMF's was discovered in the ^{12}C (1030 MeV) irradiation of emulsion at the CERN synchrocyclotron [4]. These findings stimulated the development of many theoretical models to put forward an attractive idea that copious production of IMF's may be related to a liquid-gas phase transition in nuclear matter [5, 7, 8, 9]. A recent survey of multifragmentation can be found in Ref. [10].

About a dozen sophisticated experimental devices were created to investigate this process by using heavy ion beams, which are well suited for producing extremely hot systems. But in the case of heavy projectiles, nuclear heating is accompanied by compression, fast rotation and shape distortion which may cause dynamic effects in the multi-fragment disintegration and it is not easy to disentangle all these effects and extract information on the thermodynamic properties of hot nuclear systems. The situation becomes more transparent if light relativistic projectiles are used. In this case, dynamic effects are expected to be negligible. Another advantage is that all the fragments are emitted by a single source: a slowly moving target remainder. Its excitation energy might be almost entirely thermal. Light relativistic projectiles provide therefore a unique possibility to study "thermal multifragmentation".

The time scale of the IMF emission is a crucial question for understanding this decay mode: Is it a "slow" sequential process of independent emission of IMF's or is it a new (multibody) decay mode with "simultaneous" ejection of fragments governed by the total accessible phase space? Only the latter process is usually called "multifragmentation". "Simultaneous" emission means that all fragments are liberated during a time smaller than the characteristic one $\tau_c \approx 10^{-21}$ s [11], which is the mean time for the Coulomb acceleration of fragments. During this time the IMF emission is not independent, but IMF's interact via Coulomb forces and are accelerated after freeze-out in a common electric field. The measurement of the emission time τ_{em} of IMF's (i.e., the mean time between two successive fragment emissions) is a direct way to answer the question about the nature of the multifragmentation phenomenon. The analysis of the IMF-IMF correlation function with respect to the relative velocity and also to the relative angle are two procedures for extracting information about the emission time.

By now it has been shown that thermal multifragmentation indeed takes place in collisions of light relativistic projectiles (p, $\bar{\text{p}}$, ^{3}He, ^{4}He, π^-) with a heavy target and that fragments are emitted from an expanded, excited residue after an expansion

driven by the thermal pressure [6, 12, 13, 14, 16, 17]. Deduced from the IMF-IMF correlation data, the fragment emission time is less than 100 fm/c. This value is considerably smaller than the characteristic Coulomb time. Thus, the trivial mechanism of multiple IMF emission (independent fragment evaporation) is excluded [15, 18, 19].

In this paper we present results of the experimental study of the multifragment emission induced by relativistic helium and carbon ions and compare them with our data [13] obtained for p+Au collisions. The measured fragment multiplicities, energy, charge and angular distributions are analyzed in the framework of the combined approach: Cascade Model followed by the Statistical Multifragmentation Model. Emphasis is put on the question of thermalization and on a study of a transition from a pure statistical process to a behavior showing dynamical effects.

2 The Experiment

2.1 Experimental Setup

The experiments were performed with the beams from the JINR synchrophasotron in Dubna using the modified [20] 4π-setup FASA [21]. The device consists of two main parts : First, five ΔE (ionization chambers) $\times$ E (Si)-telescopes, which serve as a trigger for the read-out of the system allowing measurement of the charge and energy distributions of IMF's at different angles. They are located at $\theta = 24°$, $68°$, $87°$, $112°$ and $156°$ to the beam direction and together cover a solid angle of 0.03 sr. Second, the fragment multiplicity detector (FMD) consisting of 64 CsI(Tl) counters (with thicknesses around 30 mg$\cdot$cm^{-2}) which covers 89% of 4π. The FMD gives the number of IMF's in the event and their spatial distribution. Thin polycrystalline CsI(Tl) films are prepared by thermal vacuum evaporation on 2 mm plexiglass backings, which are shaped as hexagons or pentagons. The light is transported onto photomultipliers of type FEU-110 by hollow metal tubes using diffuse reflection. Using such lightguides instead of solid ones made from plexiglass significantly reduces the background caused by beam halo (up to a level of several percent). Background was continuously controlled by means of a double-gate mode in processing the photomultiplier pulses. The scintillator faces were covered by aluminized Mylar (0.2 mg$\cdot$cm^{-2}) to exclude light cross talk.

A self-supporting Au target 1.5 mg/cm^2 was located in the center of the FASA vacuum chamber ($\sim$ 1 m in diameter). The following beams are used: protons at energies of 2.16, 3.6 and 8.1 GeV, ^{4}He at energies of 4 and 14.6 GeV and ^{12}C at 22.4 GeV. The average beam intensity was $7 \cdot 10^8$ p/spill for protons and helium and $1 \cdot 10^8$ p/spill for carbon projectiles with a spill length of 300 ms and a spill period of 10 s.

2.2 Analysis of Fragment Multiplicity

Using the FMD array, the associated IMF multiplicity distribution $W_A(M_A)$ is measured in events triggered by a fragment in at least one of the telescopes. The triggering probability is proportional to the multiplicity M of the event (primary IMF multiplicity). Hence, the contribution of events with higher multiplicities in $W_A(M_A)$ is enhanced. This is a reason why $W_A(M_A)$ should differ from the primary multiplicity distribution $W(M)$. Another reason is that the FMD efficiency is less than 100% and depends on the detection threshold of scintillator counters being adjusted in such a way as to reduce the admixture of particles with $Z \leq 2$ in the counting rate of IMF's up to the level $\leq 5\%$. These distributions are mutually related via the response matrix of the FASA setup $Q(M_A, M)$:

$$W_A(M_A) = \sum_{M=M_A+1} Q(M_A, M) \cdot W(M) \quad . \tag{1}$$

The response matrix includes the triggering probability, which is proportional to M, and the probability of detecting (in the FMD) M_A fragments among the remaining $M - 1$ fragments. The latter probability is described by the binomial distribution and one gets

$$Q(M_A, M) = \frac{M!}{M_A!(M - 1 - M_A)!} \varepsilon^{M_A} (1 - \varepsilon)^{M-1-M_A} \tag{2}$$

with a detection efficiency ε.

The FMD efficiency ε was calibrated as described in Ref. [20, 21]. We have the possibility to control its value experimentally using IMF coincidences in the trigger telescopes. From Eqs. (1) and (2) one finds the following relation between $< M_A >$ and the moments of the primary multiplicity distribution :

$$\frac{< M_A >}{\varepsilon} = \frac{< M^2 >}{< M >} - 1 \quad . \tag{3}$$

This expression gives the mean IMF multiplicity (without one) for events selected by the trigger.

The right-hand side of this equation can be obtained also from the coincidence rate n_{12} for IMF's in the triggering telescopes :

$$\frac{n_{12}}{n_1 p_2} = \frac{< M^2 >}{< M >} - 1 \quad . \tag{4}$$

Here n_1 is the counting rate in telescope 1, p_2 is the detection probability for a coincident fragment in the telescope 2.

The value of p_2 is largely determined by the efficiency of the second telescope ε_2 but depends also on its position (θ_2) and the relative angle θ_{12} : $p_2 = \varepsilon_2 \cdot f(\theta_1)\, g(\theta_{12})$. These last corrections are found from measured angular distributions and relative

angle correlations. Combining Eqs. (3) and (4) one gets the following relation for the FMD efficiency :

$$\varepsilon = < M_A > / \frac{n_{12}}{n_1 p_2} \quad . \tag{5}$$

There are two options for obtaining the primary multiplicity distribution $W(M)$ from the measured one $W_A(M_A)$. The first is to parameterize the $W(M)$ distribution, to fold it with the experimental filter according to Eq. (1) and then to find the parameterization parameters by fitting the result to the experimental distribution. This has been done assuming that $W(M)$ is shaped like the Fermi function, as motivated by calculations within the statistical multifragmentation model (see below).

The second option is the direct reconstruction of $W(M)$ using the inverse matrix $Q^{-1}\ (M, M_A)$:

$$W(M) = \sum_{M_A=0}^{M-1} Q^{-1}(M, M_A)\ W_A(M_A) \quad . \tag{6}$$

Both procedures give rise to similar results. In Fig. 1 the multiplicity distributions obtained for the gold target fragmentation by 14.6 GeV alphas and 22.4 GeV carbon ions are compared to those for $p(8.1 GeV) + Au$ collisions. In these cases the mean values $< M >$ are always about 2.1 – 2.2 (see Table 1) being close to that obtained by the ISIS group for ^{3}He +Au collisions at 4.8 GeV [22]. Note, these values correspond to the events with at least one IMF emitted. In this definition M is never less than 1. The mean multiplicity for all the inelastic events is smaller by the factor $(1 - P(0))$ where $P(0)$ is the probability of having no IMF in the collision.

The mean values of the IMF multiplicity can be obtained also from the counting rates of coincidences for telescopes using the relation between $< M^2 > / < M > -1$ and $< M >$ shown in Fig. 2. It was calculated for systems at different excitation energies by the Statistical Multifragmentation Model (see later) which reproduces well the IMF multiplicity distributions as is seen in Fig. 1.

3 Model Calculations

The reaction mechanism for light relativistic projectiles is usually divided into two steps. The first one consists of a fast energy-deposition stage, during which very energetic light particles are emitted and a nuclear remnant (spectator) is excited. The second one is a decay of the target spectator. The fast stage is usually described in terms of a kinetic approach. We use a refined version of the intranuclear cascade model [23] to get the distributions of nuclear remnants in charge, mass and excitation energy. The second stage can be described by multifragmentation models. The Statistical Multifragmentation Model (SMM) [24] and the Expanding Emitting

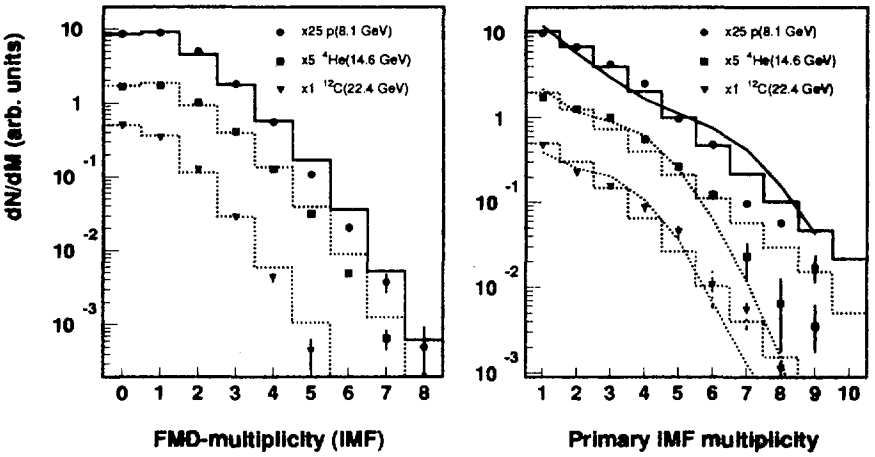

Fig.1.a) Measured IMF-multiplicity distributions (symbols) and fits with a Fermi function (folded with the experimental filter, histograms) associated with a trigger fragment for p+Au collisions at 8.1 GeV (circles, solid line), ^{4}He+Au at 14.6 GeV (squares, dashed line), and ^{12}C + Au at 22.4 GeV (triangles, dotted line). b) Symbols (same notation as in a)) represent reconstructed primary IMF distributions; Histograms are the Fermi distributions used to fit the data in the left part. The smooth lines are calculated with the RC+α+SMM model (see text).

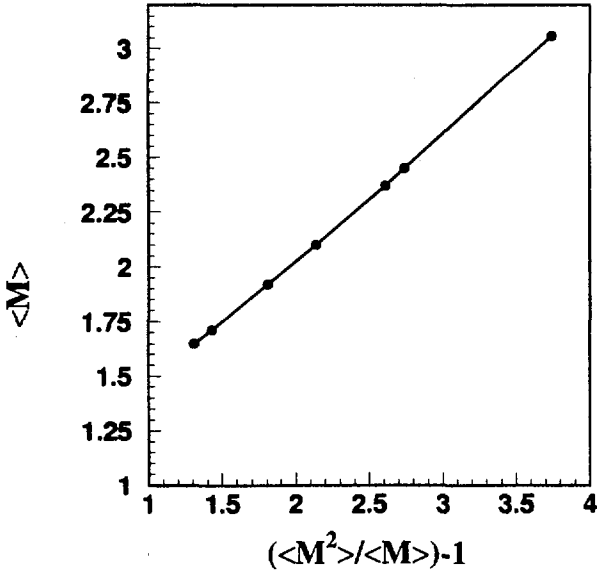

Fig.2. The relation between the moments of the IMF-multiplicity distribution according to SMM. The calculations (dots) have been made for different collision systems.

Source model (EES) [25] are employed here. It will be discussed below (sections 4.2 and 4.3) whether the assumption of thermo-equilibrium behavior is justified.

3.1 Refined Cascade Model

The Refined Cascade Model (RC) is a version of the Quark-Gluon String Model developed in Ref. [26] and extended towards intermediate energies in Ref. [27]. This is a microscopic model which is based on the relativistic Boltzmann-type transport equations and the string phenomenology of hadronic interactions. Baryons and mesons belonging to the two lowest $SU(3)$ multiplets along with their antiparticles are included. The interactions between the hadrons are described by a collision term, where the Pauli principle is imposed in the final states. This includes elastic collisions as well as hadron production and resonance decay processes. The formation time $\tau_f = 1$ fm/c for produced particles is incorporated. At moderate energies in the limit $\tau_f \to 0$, this treatment is reduced to the conventional cascade model [23].

Mean field dynamics is neglected in our consideration. However, we keep the nuclear scalar potential to be defined for the initial state in the local Thomas-Fermi approximation, changing in time only the potential depth according to the number of knocked-out nucleons. This "frozen mean-field" approximation allows us to take into account nuclear binding energies and the Pauli principle as well as to estimate the excitation energy of the residual nucleus through excited particle-hole counting. This approximation is good for hadron-nucleus or peripheral nucleus-nucleus collisions where there is no large disturbance of the mean field but it is questionable for violent central collisions of heavy ions. However, in central collisions the fraction of spectator matter is small and the available phase space for baryons is enlarged, so the role of nuclear binding and the Pauli effect can be expected to decrease.

It is traditionally assumed that after completing the cascade stage the excited residual nucleus stays in an equilibrium state. In general this is not evident. The RC includes the possibility to describe the attainment of thermodynamical equilibrium in terms of the pre-equilibrium (PE) exciton model [23, 28, 29]. During this equilibration process some pre-equilibrium particles may be emitted which will result in the change of characteristics for a thermalized residual nuclei.

Typical results of the distributions of residual masses A_R versus their excitation energies E_R in this model are shown in Fig. 3.

3.2 Statistical Multifragmentation Model

Within the SMM [24], the probability of equilibrium decay into the given channel is proportional to its statistical weight. The break-up volume determining the Coulomb energy of the system is a key parameter. It is taken as $V_b = (1 + k)A/\rho_0$, where A is the mass number of the fragmenting nucleus, ρ_0 is the normal nuclear density and k is a free parameter. In Refs. [12, 13, 18] we have shown that the break-

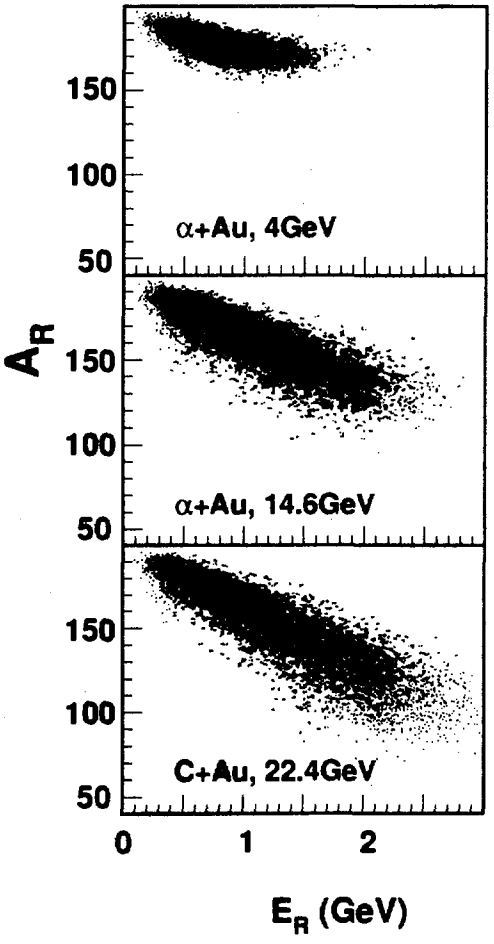

Fig.3. Distribution of residual masses A_R and excitation energies E_R after the cascade calculation for ^{4}He+Au at 4 and 14.6 GeV, ^{12}C+Au at 22.4 GeV.

up occurs at low density. To reach these density values it is assumed that the system expands before the break-up. The primary fragments may be excited and their deexcitation is taken into account to get final IMF distributions. Figure 4 shows the IMF multiplicity as a function of the excitation energy calculated for $k = 2$ and $k = 5$ which corresponds to the freeze out densities about $\approx 1/3\,\rho_0$ and $1/6\,\rho_0$, respectively. The calculations have been performed with the RC+SMM combined model for ^{4}He+Au collisions at 14.6 GeV. The fragment multiplicity rises with excitation energy up to a maximum and then decreases due to vaporization of the overheated system. This so-called "rise and fall" of multifragmentation is well visible in the figure and was first demonstrated experimentally by the ALADIN group for the collisions of ^{197}Au at 600 MeV/nucleon with Al and Cu targets [30].

The choice of the break-up density only slightly influences $< M >$. The kinetic energies of fragments are more affected because they are determined mainly by the Coulomb field in the system depending noticeably on its size. The implementation of a larger value of parameter ($k = 5$) results in the underestimation of the fragment kinetic energies compared to the data [31]. In further calculations we use $k = 2$ based on our analysis of the correlation data [18].

All calculations are performed in an event-by-event mode.

4 Results and Discussion

4.1 Fragment multiplicity and excitation energy of the system

The mean IMF multiplicities, measured and calculated, are shown in Fig. 5 as a function of the total beam energy for various projectiles. The data exhibit a saturation in $< M >$ for energies above ~ 6 GeV in good agreement with findings of previous work [13, 32, 33]. This so-called limiting fragmentation may be caused by a saturation of the residual excitation energy while the fragment multiplicity is strongly energy dependent. Other possible reasons for the saturation effect are discussed in [32].

The dashed line in Fig. 5 is obtained by means of the combined RC+SMM model. The calculated mean multiplicities are significantly higher than the measured ones except for the lowest beam energy. This fact indicates that the model overestimates the residue excitation energy. May the pre-equilibrium light particle emission be responsible for this discrepancy? The inclusion of the pre-equilibrium emission after the cascade stage (RC+PE+SMM) results in a significant decrease of the excitation energy of the fragmenting target spectator and reduces the mean IMF multiplicity (dotted line in Fig. 5). However, the multiplicity reduction turns out to be too large for $E_{proj} < 8$ GeV predicting $< M >$ to be smaller than the measured ones. One should note that though the calculated value of $< M >$ for the p(8.1 GeV)+Au collisions coincides with the experiment, the model-predicted fragment kinetic energies in this approach are significantly lower than the measured ones, as shown in [13].

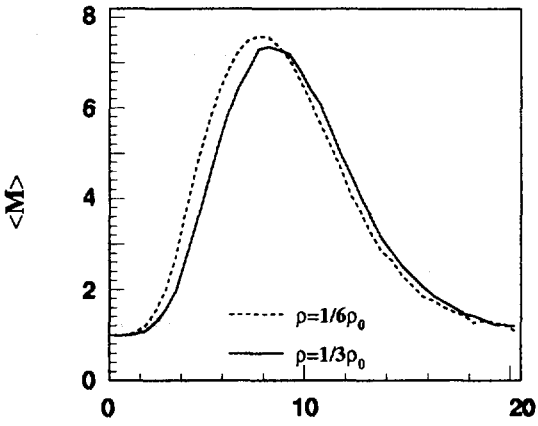

Fig.4. Mean fragment multiplicities as a function of the thermal excitation energy according to SMM, calculated for the freeze-out densities about $\approx 1/3\,\rho_0$ and $1/6\,\rho_0$.

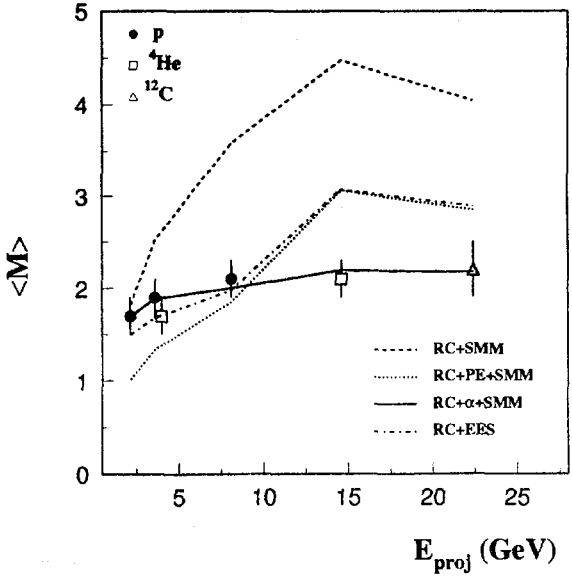

Fig.5. Mean IMF multiplicities (for events with at least one IMF) as a function of beam energy. The points are experimental data. Dashed and dotted lines are drawn through the values calculated with RC+SMM and with RC+PE+SMM at the beam energies used. The solid line is obtained with the use of RC+α+SMM and the dash-dotted one from RC+EES. For simplicity, only one line is drawn for a given model calculation neglecting the dependence on projectile mass.

Because the IMF energies are determined essentially by the Coulomb field of the source, the RC+PE+SMM model underestimates the charge Z of a target residue. In addition, at higher ^{4}He-beam energies, the drop in excitation energy after the pre-equilibrium emission is not even strong enough to get the observed fragment multiplicities. All these facts may testify to another possible mechanism for the energy loss before the IMF emission.

Calculations with the EES model [25] have been performed using the same characteristics of the RC-remnants. As can be seen in Fig. 5, the obtained values (RC+EES) of the mean fragment multiplicities are in accordance with the data for the beam energies below 10 GeV, but there is a disagreement between theory and experiment for higher energies.

We conclude that neither RC nor RC+PE are able to describe the properties of the target spectator over a wide range of projectile energies. One should look for an alternative approach.

An example of an empirical approach to this problem is given in paper [34] devoted to an analysis of the experimental data on multifragmentation in the reactions of ^{197}Au on C, Al, Cu and Pb targets at E/A=600 MeV. The parameterized relations (with 7 parameters) were developed to get the mass and energy distributions of highly exited thermalized nuclear systems formed as the spectator parts of the colliding nuclei. This distribution was used as an input for the SMM calculations, and parameters were adjusted to fit the experimental results on the IMF multiplicity distributions and their yield. It should be stressed that the suggested parameterization is specific for the considered reaction.

In our approach we start with the results of the cascade calculation and modify them empirically. In paper [35] the excitation energies of the cascade remnants have been reduced by a factor α (see below) on an event-by-event basis keeping the mass unchanged. It is motivated by a guess that the "frozen mean field" approximation in the cascade calculation may result in an overestimation of the high energy tail of the distribution. The mean IMF multiplicities obtained by this procedure are in accordance with the data for p+Au collisions in the range of projectile energies (2-8) GeV.

At the next step of our analysis of the same reactions [13], the drop in excitation energy is accompanied by a mass loss. This combination holds both for preequilibrium emission in the spirit of the exciton model [29] and for particle evaporation during the expansion, as considered by the EES model [25].

In the present paper we follow the last approach. The excitation energies E_R^{RC} of the residual nuclei A_R given by the RC code are reduced by a fitting factor α to get the excitation energy of a multifragmenting state E_{MF}, *i.e.* $E_{MF} = \alpha \times E_R^{RC}$. In other words, the drop in the excitation energy is equal to $\Delta E = (1-\alpha)E_R^{RC}$. As is known from the cascade calculations, E_R^{RC} is proportional to the nucleon loss during the cascade ΔA^{RC}, so $\Delta E = (1-\alpha)\varepsilon_1 \Delta A^{RC}$, where ε_1 is a mean excitation energy per ejected cascade nucleon. The loss in mass ΔA corresponding to the this

drop in the excitation energy is $\Delta A = \Delta E/\varepsilon_2$, where ε_2 is the mean energy removed by a nucleon. Assuming $\varepsilon_2 \approx \varepsilon_1$ one gets $\Delta A = (1-\alpha)\Delta A^{RC}$. We denote this empirical combined model as RC+α+SMM.

In the earlier paper [13] for p+Au collisions, a simple relation could be applied

$$\alpha = \frac{< M_{exper} >}{< M_{RC+SMM} >}$$

because the range of the excitation energies corresponded to the rising part of the energy dependence of $< M >$ shown in Fig. 4. However, due to the rise-and-fall effect in $< M >$, this relation fails for heavier projectiles. For these systems the values of α are empirically adjusted to reproduce the measured mean IMF multiplicities. The charge, mass and energy characteristics of fragmenting nuclei resulting from this fitting procedure are presented in Table 1 for various colliding systems. The corresponding values for the p+Au case differ slightly from those given in Ref. [13] because a new cascade code is used here. The values of the α parameter can be found in Table 1 by calculating the ratio E_R(RC+α+SMM)/E_R(RC+SMM) which gives 0.93, 0.76 and 0.53 (for p+Au), 0.49 and 0.25 (for He+Au), 0.22 (for C+Au), respectively.

As follows from the given values of the α parameter, a rather large decrease of the residual excitation energy is required by this empirical procedure to reproduce the observed saturation effect in $< M >$ which is caused mainly by a saturation in E_{MF}. This is illustrated in Fig. 6 which shows the population of events in the M - E_{MF}/A plane calculated in both the RC+SMM (left panel) and RC+α+SMM (right panel) scenarios. According to the first approach the excitation energy distribution is rather wide and populates states along both the rising and the falling parts of the multiplicity curve. In the RC+α+SMM scenario the events are mainly situated in the rising part hardly approaching the region of maximal values of the IMF multiplicity that is in agreement with the measured data.

Note that the excitation energies of fragmenting nuclei given in Table 1 are thermal ones by definition. As it is shown in Chap. 4.3 for both C(22.4 GeV)+Au and He(14.6 GeV)+Au collisions, the systems at break-up have also a collective expansion energy, which is estimated to be ~100-130 MeV for both cases. The total excitation energy, E^*_{MF}, for these cases is in fact larger by that value than the values shown in Table 1. This is taken into account in Fig. 7, which presents the calculated values of the mean residual excitation energies and mass numbers. The total excitation energy E^*_{MF} is slightly changing with increasing incident energy. At the same time, the excitation energy per nucleon rises while the residual mass is decreasing and the mean IMF multiplicity is almost constant.

It would be of interest to compare the extracted masses and excitation energies of fragmenting nuclei to those obtained by the EOS collaboration for Au(1 GeV/nucleon)+C collisions (in inverse kinematics) [36]. In this paper the mass and energy balance relations are applied with use of the measured kinetic energies of all

E_{inc} (GeV)	Proj	Exper. M_{IMF}	Calculations							Model
			M_{IMF}	Z_R	A_R	Z_{MF}	A_{MF}	E_R	E_{MF}	
2.16	p	1.7±0.2	1.82	77	189	76	185	310	589	RC+SMM
			1.02	72	176	62	145	119	266	RC+PE+SMM
			1.69	77	188	75	183	288	564	RC+α+SMM
3.6	p	1.9±0.2	2.52	76	187	74	181	371	676	RC+SMM
			1.34	70	171	55	134	148	385	RC+PE+SMM
			1.89	75	184	73	175	282	568	RC+α+SMM
8.1	p	2.1±0.2	3.58	75	183	73	175	488	808	RC+SMM
			1.85	68	167	53	128	177	462	RC+PE+SMM
			2.0	72	176	67	158	259	529	RC+α+SMM
4.0	^{4}He	1.7±0.2	3.89	75	184	73	177	484	836	RC+SMM
			1.56	68	167	54	130	176	428	RC+PE+SMM
			1.77	73	177	69	161	238	502	RC+α+SMM
14.6	^{4}He	2.2±0.2	4.47	71	173	66	159	723	1132	RC+SMM
			3.06	63	153	48	116	377	824	RC+PE+SMM
			2.19	64	154	48	103	183	404	RC+α+SMM
22.4	^{12}C	2.2±0.3	4.04	67	163	64	153	924	1216	RC+SMM
			2.85	60	146	47	113	638	1026	RC+PE+SMM
			2.17	59	139	41	86	207	415	RC+α+SMM

Table 1: The calculated properties of nuclear remnants from *proj* + Au collisions. The M_{IMF} is the mean number of IMF's for events with at least one IMF and Z_R, A_R, E_R are the mean charge, mass number and excitation energy (in MeV), respectively, averaged over all inelastic collisions, while similar quantities Z_{MF}, A_{MF}, E_{MF} are averaged only over residues decaying by IMF emission.

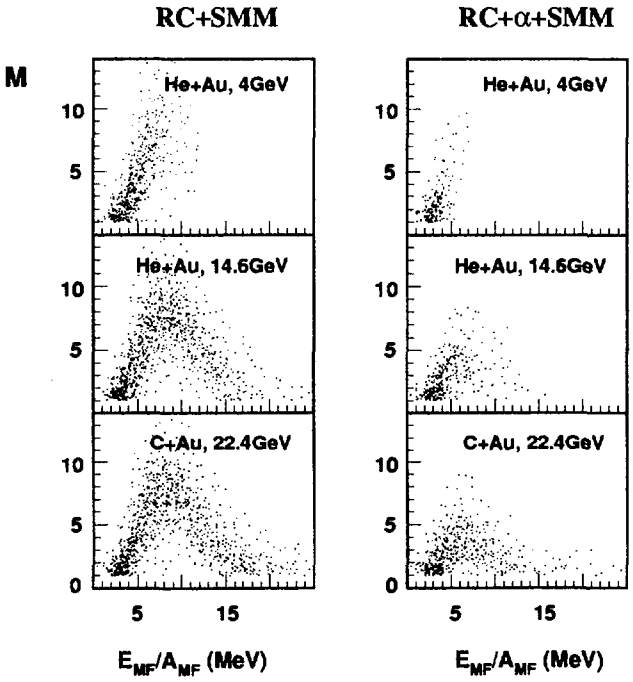

Fig.6. The calculated event distribution in M-E_{MF}/A_{MF} plane: RC+SMM model (left) and RC+α+SMM approach (right).

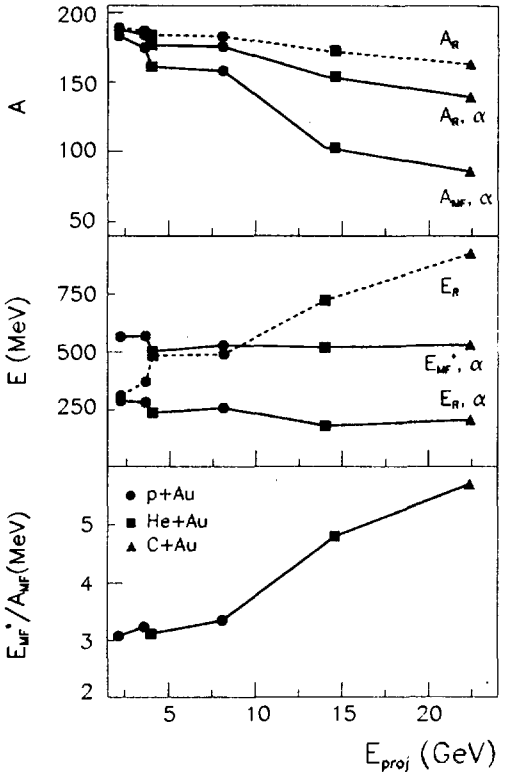

Fig.7. Mean values of the remnant excitation energies and mass numbers according to Table 1: E_R and A_R are for averaging over all inelastic collisions, E_{MF}, A_{MF} are for fragmenting residues. The calculations with RC+α+SMM are marked by "α".

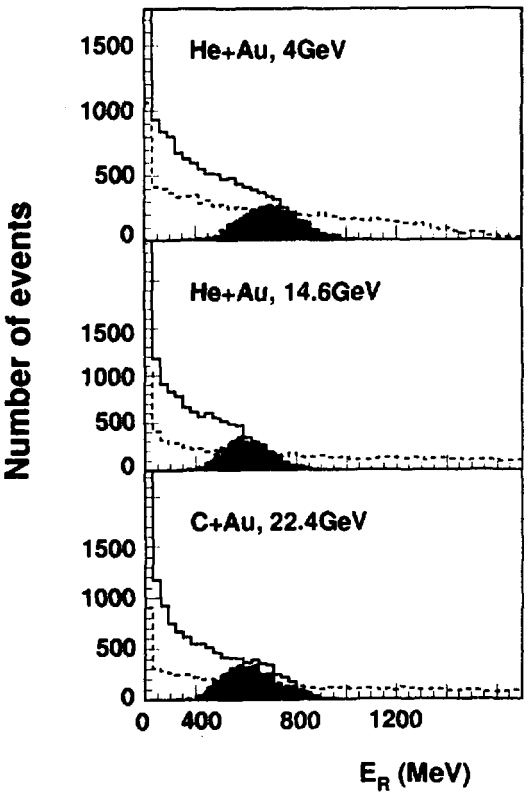

Fig.8. Distribution of excitation energies obtained with RC (dashed lines), with RC+α (solid lines) and the fraction decaying by multifragmentation according to RC+α+SMM (hatched area).

the outgoing charged particles after separating from the prompt stage of the reaction. The neutron contribution was taken into account on the basis of cascade and statistical model simulations. The inclusive data were not presented there and only the values, corresponding to the mean IMF multiplicity were used for the comparison. Our value of E^*_{MF}/A_{MF} is close to that from Ref. [36] if the collective energy is added. As to the mean mass A_{MF}, the value obtained in the present work (≈ 90) is remarkably lower, being caused by the larger mass loss induced by the projectile with twice the energy.

Some examples of the excitation energy distributions are displayed in Fig. 8. The IMF emission takes place on the tail of the distributions, therefore the mean excitation of the fragmenting nuclei is much larger than that averaged over all the target spectators.

In Fig. 9 the obtained energy E^*_{MF} is confronted with the values predicted by the EES model [25]. The excitation energy after the cascade stage is taken as initial one for the process of the energy (and mass) loss during the expansion of the system. Data for p+Au collisions are close to the predicted values if the excitation energy was corrected according to the above-discussed procedure, while in all the cases for the ^{4}He and ^{12}C beams the EES model overestimates the excitation energy after expansion. This may be a sign of a possible contribution of an additional mechanism of the energy loss (e.g. pre-equilibrium emission).

4.2 Angular and charge distributions

Now let us consider the question of thermalization of the system at break-up. To check how close the emitting system is to thermal equilibrium, the plot of the fragment probability distribution in terms of the longitudinal-transverse velocity components is presented in Fig. 10 for the ^{4}He+Au and C+Au collisions. The symbols correspond to the constant invariant cross sections taken for emitted carbon fragments in the energy range above the spectral peak. The lines connecting experimental points form circles demonstrating an isotropic emission in the frame of a moving source indicating that the fragment emission proceeds from a thermalized state. The center positions of the circles determine the source velocity, β_{source}. The mean values of β_{source} are in the range of (0.01-0.02)c to be close to an estimate within the RC+α+ SMM model for all the cases except ^{4}He+Au at 4 GeV, where calculations underestimate the source velocity. The calculated mean β_{source} values are $0.76 \cdot 10^{-2}$, $1 \cdot 10^{-2}$, $1.36 \cdot 10^{-2}$ and $1.7 \cdot 10^{-2}$ for p(8.1 GeV)+Au, ^{4}He(4 GeV), ^{4}He(14.6 GeV)+Au and C(22.4 GeV)+Au collisions respectively. The variation of β_{source} with the IMF velocity, β_{IMF} is shown in Fig. 11.

The fragment angular distribution in the laboratory system exhibits a forward peak caused by the source motion as shown in Fig. 12 for carbon fragments. The data are well reproduced by the model calculations except for the helium beam case at the lowest energy. The measured distribution here is more forward peaked

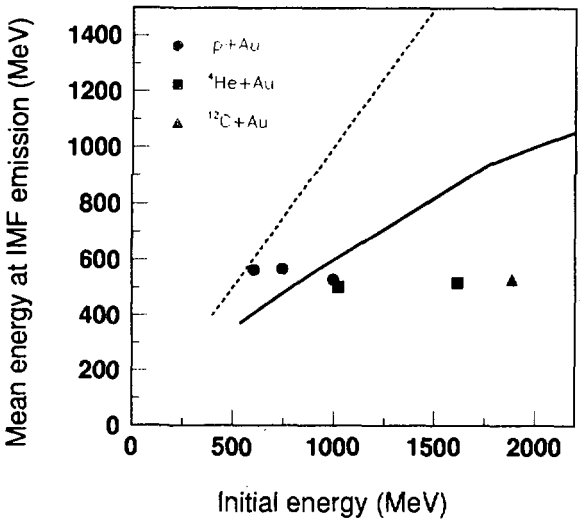

Fig.9. The loss in the excitation energy during the expansion calculated by RC+EES model (solid line) is compared with the empirically deduced drop. The dashed line represent the initial energy (after RC stage). Points are data for proton (dots), helium (squares) and carbon (triangle) beams.

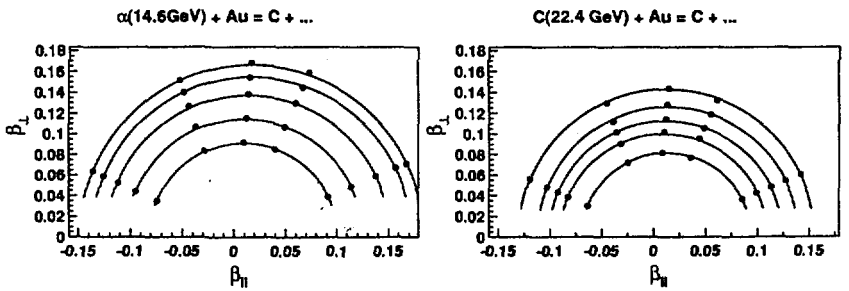

Fig.10. Transverse versus longitudinal velocity plot for emitted carbon isotopes produced in ^{4}He (14.6 GeV) and ^{12}C (22.4 GeV) collisions with a Au target. Circles are drawn through points of equal invariant cross section corresponding to isotropic emission of the fragments in the moving source frame.

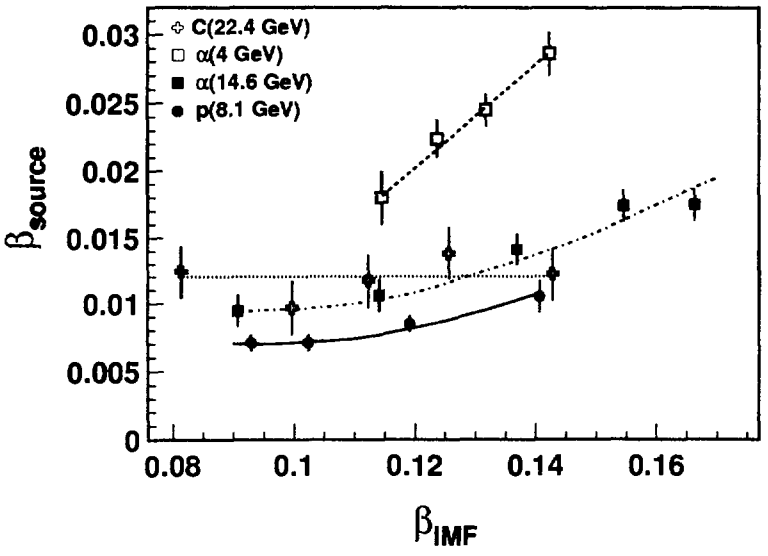

Fig.11. The source velocities β_{source} as a function of fragment velocity β_{IMF} for p+Au, ^{4}He+Au and ^{12}C+Au collisions.

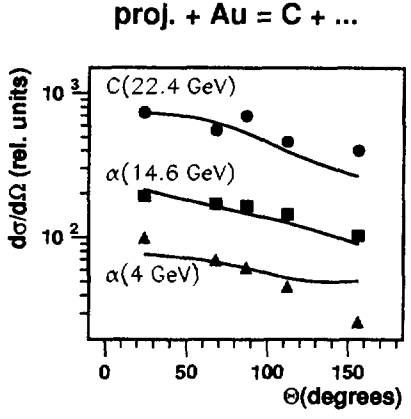

Fig.12. Angular distributions of carbon (in laboratory system) for ^{4}He+Au and ^{12}C+Au collisions. The lines are calculated using the RC+α+SMM approach.

which may be considered as an indication that the momentum transfer is larger than predicted.

The charge distributions of IMF's are shown in Fig. 13. The calculation results for the RC+α+SMM scenario agree nicely with the data. The general trend of the IMF charge (or mass) distributions is well described by a power law $Y(Z) \sim Z^{-\tau}$. The obtained values of the exponent are $\tau = 1.9 \pm 0.1$, 2.0 ± 0.1 and 2.1 ± 0.1 for helium beam of 4 GeV, 14.6 GeV and carbon projectiles, respectively (Fig. 13, right panel).

In earlier papers on multifragmentation [5, 38] the power-law behavior of the IMF yield was interpreted as an indication of the proximity of the decaying state to the critical point for the liquid-gas phase transition in nuclear matter. This was simulated by the application of the classical Fisher's droplet model [40], which predicted a pure power-law droplet-size distribution with τ=2-3 at the critical point. According to Ref. [41] the fragmenting system is not very close to the critical point. Now, the power law is well explained at temperatures far below the critical point. As seen in Fig. 13, the pure thermodynamical Statistical Multifragmentation Model predicts that the IMF charge distribution is very close to a power law at the freeze out temperatures of 5–6 MeV, while the critical temperature (i.e. where the surface tension vanishes) is $T_c = 18$ MeV. In Ref. [42], it was shown also that several results concerning the fragment size distribution can be rendered well by use of the kinetic model of condensation beyond the vicinity of the liquid-gas critical point.

Thermal multifragmentation can be considered as a first order phase transition of nuclear matter inside a spinodal region characterized by a liquid-gas phase instability. Indeed, it is proved experimentally that fragmentation takes place after expansion driven by thermal pressure[12, 13, 14], and the decomposition time is short (less than 100 fm/c) [15, 18, 19]. In fact, the final state of this transition looks like a nuclear fog [39] : liquid drops of IMF's surrounded by a gas of nucleons and light clusters, d, t and α-particles. This interpretation is in the line of the Statistical Multifragmentation Model [43]. Later it was employed in other approaches (see, for example [44].)

4.3 Energy spectra of fragments

In general, the kinetic energy of fragments is determined by four terms: thermal motion, Coulomb repulsion, rotation, and collective expansion energies of the system at freeze out, $E = E_{th} + E_C + E_{rot} + E_{flow}$. The additivity of the first three terms is quite obvious. For the last term, its independence from the others may be considered only approximately when the evolution of the system after freeze-out is driven only by the Coulomb force. The Coulomb term is significantly larger than the thermal one. It was shown in Ref. [18] that for ^{4}He (14.6 GeV)+Au the Coulomb part of the mean energy of the carbon fragment is three times larger than thermal energy. These calculations were performed within the RC+SMM scenario, where the volume

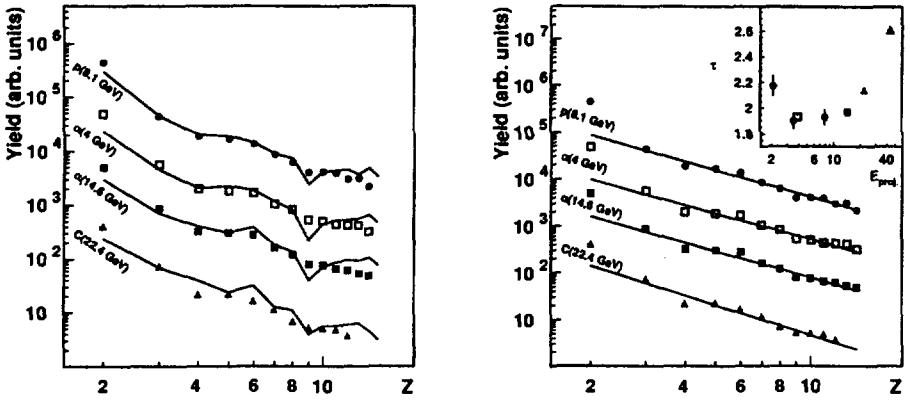

Fig.13. Fragment charge distributions obtained at $\theta = 89°$ for p+Au at 8.1 GeV (top), ^{4}He+Au at 4 GeV, ^{4}He+Au at 14.6 GeV and ^{12}C+Au at 22.4 GeV. The lines (left side) are calculated by RC+α+SMM (normalized at Z=3). The power law fits are shown on the right panel with τ-parameters given in the insert as a function of the beam energy. The last point in the insert is for ^{12}C+Au collisions at 44 GeV (from a preliminary experiment).

emission of fragments from a diluted system was taken into consideration.

The contribution of collective flow for p+Au collisions at 8.1 GeV incident energy was estimated in Ref. [13]. This was done by comparing the measured IMF spectra with the calculated ones in the framework of the SMM which includes no flow. This analysis did not reveal any significant enhancement in the measured energy spectra restricting the mean flow velocity by the value of $v_{flow} < 0.02\ c$. For the case of heavy-ion collisions, the collective flow has been observed and it is the most pronounced in central Au+Au collisions [46]. In this respect it would be quite interesting to analyse the fragment spectra from He+Au and C+Au collisions looking for a possible manifestation of collective flows. The carbon spectra for proton-, helium- and carbon-induced collisions on the Au target are presented in Fig. 14. The calculated carbon spectrum for p+Au collisions (at 8.1 GeV) is consistent with the measured one. A similar situation occurs with ^{4}He+Au collisions at 4 GeV, but not with ^{4}He(14.6 GeV)+Au and ^{12}C+Au interactions: the measured spectra are harder than the calculated ones.

The mean kinetic energies per fragment nucleon are given in Fig. 15, only statistical errors are shown. There is a remarkable enhancement in the reduced kinetic energy for light fragments from He+Au and C+Au collisions as compared to the p(8.1 GeV)+Au case. The calculated values of the mean fragment energies (shown by lines) are obtained with the RC+α+SMM model by multibody Coulomb trajectory calculations on an event-by-event basis. In the initial state all charged particles are assumed to have a thermal velocity only. The measured energies are close to the calculated ones for p+Au collisions in the range of the fragment charges between 4 and 9. However, for the ^{4}He+Au and ^{12}C+Au interactions the experimental data are definitely above the calculated values.

The observed deviation cannot be attributed to an angular momentum effect. To estimate the rotational part of energy E_{rot}, let us consider the uniform classical rotation of the system with mass number A and total rotational energy E_L. The mean rotational energy of fragment with mass A_{IMF} is equal to

$$< E_{rot} > /A_{IMF} = \frac{5}{3} < \frac{E_L}{A} > \frac{< R_Z^2 >}{R_{sys}^2} \qquad (7)$$

where R_Z and R_{sys} are the radial coordinate of a fragment and radius of the system, respectively. According to the RC calculations for C+Au collisions, the mean angular momentum of the target spectator is $L = 36\hbar$. It might be reduced by a factor of 1.5 due to the mass loss along the way to the freeze out point. Finally $< E_L >$ is estimated to be only 5 MeV and $< E_{rot} > /A_{IMF} \approx 0.04$ MeV/nucleon, which is by an order of magnitude smaller than the energy enhancement for light fragments. So, we believe that this enhancement is caused by the expansion of the system, which is assumed to be radial, as the velocity plot (Fig. 10) does not show any significant deviation from the circular symmetry.

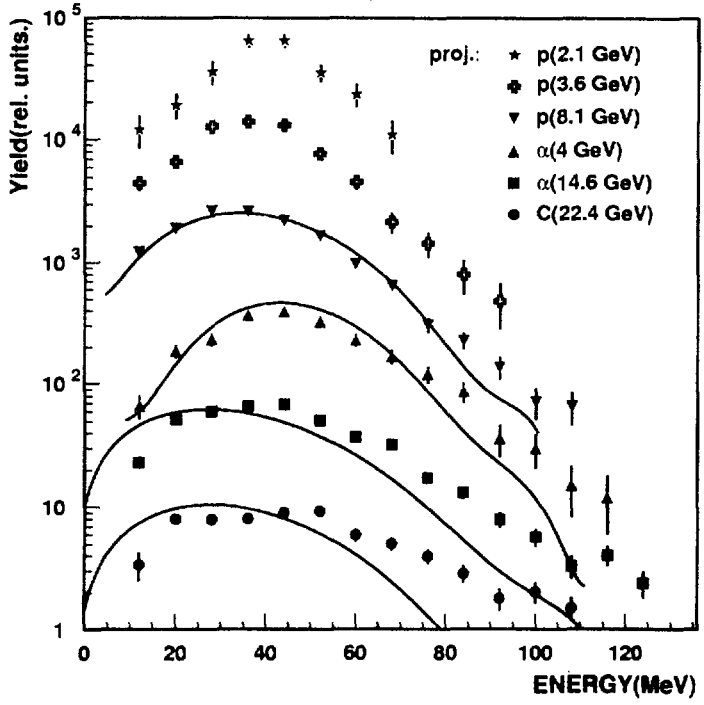

Fig.14. Energy distribution of carbon isotopes obtained for different collisior systems at $\theta = 89°$. The lines are calculated with the RC+α+SMM model assum ing no flow.

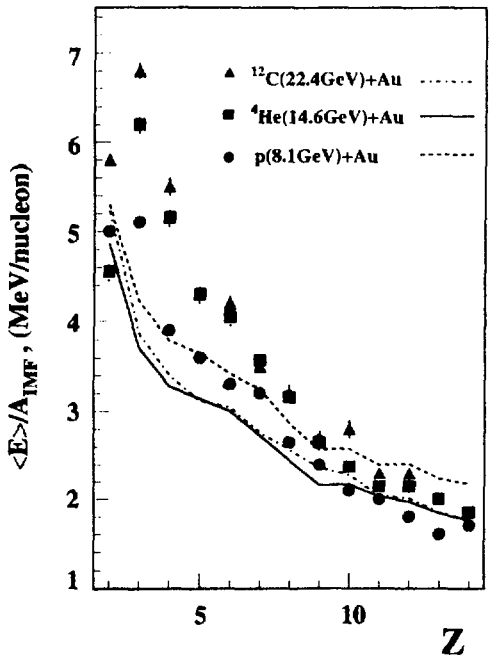

Fig.15. The mean kinetic energies per nucleon of outgoing fragments measured at $\theta = 89°$ for p(8.1 GeV), ^{4}He (14.6 GeV) and ^{12}C (22.4 GeV) collisions with Au. The lines are calculated using RC+α+SMM and assuming no flow.

An estimate of the fragment flow energy may be obtained as a difference between the measured IMF energies and those calculated without taking into account any flow in the system. This difference for C+Au collisions is shown in Fig. 16. The error bars include both statistical and systematic contributions. The latter one is related to the calibration of the energy scale and is estimated to be ~5%. In an attempt to describe the data we modified the SMM code in RC+α+SMM by the inclusion of a radial velocity boost for each particle at freeze out. In other words, a radial expansion velocity was superimposed on the thermal motion in the calculation of the multibody Coulomb trajectories. A self similar radial expansion is assumed, where the local flow velocity is linearly dependent on the distance of the particle from the centre of mass. The expansion velocity of particle Z located at radius R_Z is given by the following expression:

$$\vec{v}_{flow}(Z) = v^0_{flow} \cdot \frac{\vec{R}_Z}{R_{sys}} \tag{8}$$

where v^0_{flow} is the radial velocity on the surface of the system. Note, that in this case the density distribution is changing in a dynamic evolution by a self-similar way being a function of the scaled radius R_Z/R_{sys}. The use of the linear profile for the radial velocity is motivated by the hydrodynamic model calculations for an expanding hot nuclear system (see for example Ref. [45]). The value of v^0_{flow} has been adjusted to describe the mean kinetic energy measured for the carbon fragment. The results are also presented in Fig. 16 as a difference of calculated fragment energies obtained for v^0_{flow}=0.1c and v^0_{flow}=0. The data deviate significantly from the calculated values for Li and Be. This may be caused in part by the contribution of particle emission during the early stage of expansion from the hotter and denser system. It is supported by the fact that the extra energy of Li fragments with respect to the calculated value is clearly seen in Fig. 15 even for proton-induced fragmentation, where no significant flow is expected. This peculiarity of light fragments has been noted already by the ISIS group for ^{3}He+Au collisions at 4.8 GeV [22].

As to fragments heavier than carbon, the calculated curve in Fig. 16 is above the data and only slightly decreases with increasing fragment charge. In general, such a behaviour should be expected. The mean fragment flow energy is proportional to $< R_Z^2 >$. This value is only slightly changing with fragment charge in the SMM code due to the assumed equal probability for fragments of a given charge to be formed at any point of the available break-up volume. This assumption is a consequence of the model simplification that considers the system as uniform with $\rho(r)$=const for $r \leq R_{sys}$. The discrepancy between the data and the calculations in Fig. 16 indicates that a uniform density distribution is not fulfilled. The dense interior of the expanded nucleus is favored over for the appearance of larger IMF's, if fragments are formed via the density fluctuations. This observation is in accordance also with the analysis of the mean IMF energies performed in Ref. [13, 38] for proton induced

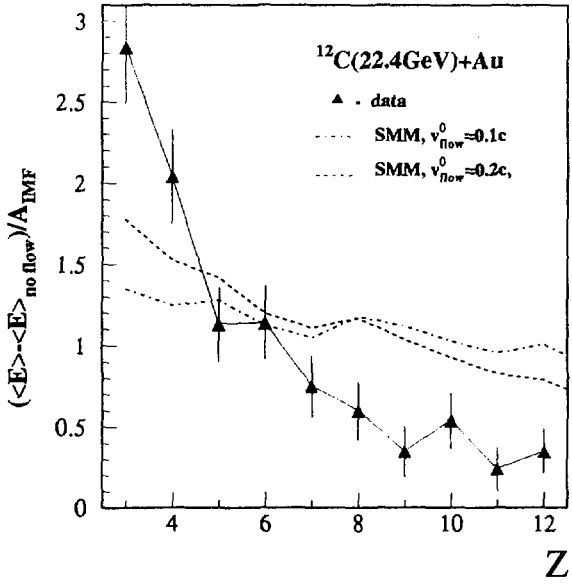

Fig.16. Flow energy per nucleon (triangles) obtained as a difference of the measured fragment kinetic energies and the values calculated under assumption of no flow in the system. The lines represent calculations assuming a linear radial profile of the expansion velocity with $v^0_{flow} = 0.1$ c (dotted line) and quadratic profile with $v^0_{flow} = 0.2$ c (dashed line).

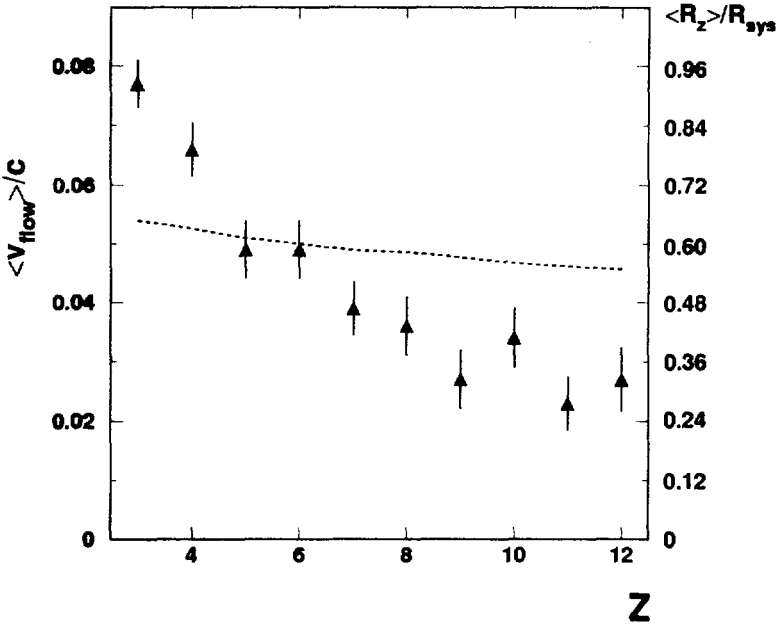

Fig.17. Experimentally deduced mean flow velocities (triangles) for ^{12}C+Au collisions as a function of the fragment charge (left scale), and the mean relative radial coordinates of fragments (right scale), obtained under the assumption of a linear radial profile for the expansion velocity. Dashed line shows the mean radial coordinates of fragments according to the SMM code.

fragmentation. It is seen also in Fig. 15, that For p+Au collisions the measured energies are below the theoretical curve for fragments heavier than Ne. This may be explained by the preferential location of the heavier fragments in the interior region of the freeze out volume, where the Coulomb field is reduced. The deviation of data from the calculations becomes less but still remains, if one assumes the quadratic radial profile of the expansion velocity. The result of such calculation shown in Fig. 16 is obtained with v^0_{flow}=0.2c, which has been choosen to be close to the data at Z=6. The interesting feature of a reduced flow energy for heavier fragments is observed also for central heavy ion collisions (see review paper [49]). This effect is increasingly important at energies $\leq$100 AMeV, and that is in accordance with our suggestion on its relation to the density profile of the hot system at freeze out.

For the estimation of the mean flow velocities of fragments, the difference between the measured IMF energies and calculated ones (no flow) has been used. The results are presented in Fig. 17. The values for Li and B are considered as upper limits because of the possible contribution of the precquilibrium emission. The corresponding values of $< R_Z > /R_{sys}$, obtained under the assumption of a linear radial profile for the expansion velocity, can be read on the right-hand scale of the figure. Again the reduced radius value for the carbon fragment is chosen to coincide with the calculated one. The dashed line shows the mean radial coordinates of fragments according to the SMM code. As it has been noted above, the calculated values of $< R_Z > /R_{sys}$ are only slightly decreasing with Z in contrast with the data.

Effects of the radial collective energy for 1· A GeV Au+C collisions (in the inverse kinematics) were considered in [47] by analyzing the transverse kinetic energies K_t of fragments with $Z = 2-7$. This was done for two charged-particle multiplicity bins, corresponding to peripheral (M1) and central (M3) collisions. The Berlin statistical model code [48] was used with inclusion of a radial velocity chosen properly to account for the experimental values of $< K_t >$. In the case of peripheral collisions the obtained expansion velocities are close to those given in Fig. 17, but the corresponding mean IMF multiplicities (in our definition) are lower than 1.5. For central collisions ($< M_{IMF} > \simeq 4$) the expansion velocities are ~ 1.5 times higher. It would be desirable to compare our data with those for the intermediate case (bin M2), which are unfortunately not available. Making an interpolation, one may see that our analysis gives slightly lower values of $v_{flow}(Z)$ as compared to Ref. [47]. This may be caused by the fact that the MMMC-model [48] underestimates the Coulomb part of the fragment kinetic energy (see [31]) as the freeze-out density used is too small ($\rho_f = 1/6\rho_0$).

The total expansion energy can be estimated by integrating the nucleon flow energy (taken according to Eq. (8)) over the available volume at freeze out. For a uniform system one gets :

$$E^{tot}_{flow} = \frac{3}{10} A \cdot m_N \, (v^0_{flow})^2 \, (1 - r_N/R_{sys})^5 \qquad (9)$$

where m_N, r_N are the nucleon mass and radius. For ^{12}C+Au collisions it gives $E^{tot}_{flow} \simeq (100 - 130)$ MeV, corresponding to a flow velocity at the surface of 0.1c. Similar results are obtained for ^{4}He(14.6 GeV)+Au collisions.

5 Conclusions

The emission of intermediate mass fragments has been studied for the reactions p(2.1, 3.6 and 8.1 GeV) + Au, ^{4}He(4 and 14.6 GeV) + Au and ^{12}C(22.4 GeV) + Au. The measured IMF multiplicities (with at least one IMF) saturate at a value around 2 for incident energies above 6 GeV independent of projectile size. The angular distributions of the IMF's are slightly forward peaked; the yield distributions of parallel versus perpendicular velocities exhibit circular symmetry. These results show that the IMF's are emitted from a source that moves with a rather low velocity (0.01 - 0.02) c. These findings support the interpretation of "thermal multifragmentation", a break-up of an expanded system.

Model calculations for the IMF multiplicities using a two-stage concept with a cascade followed by a statistical multifragmentation model, fail to describe the measured values. This might originate partly from too high an excitation energy predicted by the cascade model used. Taking into account pre-equilibrium particle emission before attainment of thermal equilibrium in the system decreases the number of IMF's but nevertheless still can not predict the observed multiplicity saturation. The employment of the Expanding Emitting Source model also fails to reproduce the measured multilplicities over the whole available energy range. Only if one applies an empirical modification of the calculated excitation energies E_R and residual masses A_R after the cascade used as input for the SMM calculations, can the IMF multiplicity saturation effect be reproduced. This study shows that the widely used approach of dividing the nuclear multifragmentation process into two distinct stages is much oversimplified.

The energy spectra of the IMF's turn out to be very sensitive observables. In p + Au collisions, the energy spectra are well described by the empirically modified cascade-SMM calculations. However, for ^{4}He and ^{12}C induced reactions the number of higher energy IMF's is larger than given by the calculations. This effect is not caused by any variation of the residual masses. We attributed this observation to the occurrence of collective (expansion) flow in the system possibly caused by a higher thermal pressure. Assuming a linear radial profile of flow velocity, its value at the surface is estimated to be around 0.1c both for ^{4}He and ^{12}C induced reactions. However, a detailed inspection of the variation of the kinetic energies of the fragments reveals that the flow velocities are not constant. This is in contrast to expectations which assume equal probability for forming fragments in systems with uniform density. The discrepancy between the extracted flow velocities and the simple assumption indicates that heavier fragments are formed more in the interior

of the system possibly due to a density gradient.

This study of multifragmentation using a range of projectiles, from protons to light nuclei, seems to be quite attractive giving new information on the various aspects of multifragmentation from a "thermal decay" to a disintegration governed by the dynamics of the collision.

The authors are thankful to Profs. A.Hrynkiewicz, A.M.Baldin, N.A.Russakovich and S.T.Belyaev for support. The research was supported in part by Grant No 00-02-16608 from Russian Foundation for Basic Research, by Grant No 2P03 12615 from the Polish State Committe for Scientific Research, by Grant No 94-2249 from INTAS, by Contract No 06DA453 with Bundesministerium fuer Forschung und Technologie and by US National Science Foundation.

References

[1] E. Schopper, Naturwissenschafter 25 (1937) 557.

[2] I.I. Gurevich et al., Dokl. Akad. Nauk SSSR 18 (1938) 169.

[3] O.V. Lozhkin, N.A. Perfilov, Zh. Eksp. i Teor. Fiz. 31 (1956) 913.

[4] B. Jacobsson et al., Z. Phys. A307 (1982) 293.

[5] P.J. Siemens, Nature 305 (1983) 410.

[6] S.J. Yennello et al., Phys. Rev. Lett. 67 (1991) 671.

[7] H.R. Jaqaman et al., Phys.Rev. C27 (1983) 2782; C29 (1984) 2067.

[8] M.W. Curtin et al., Phys. Lett. B123 (1983) 289.

[9] J.H. Rose et al., Phys. Rev. Lett. 53 (1984) 289.

[10] "Multifragmentation", Proc. of Int. Workshop XXVII on Gross Properties of Nuclei and Nuclear Excitations, Hirschegg, Austria, Jan. 17-23, 1999, Edited by H.Feldmeier, J.Knoll, W.Nörenberg, J.Wambach, GSI, Darmstadt, 1999.

[11] O. Shapiro, D.H.E. Gross, Nucl. Phys. A573 (1994) 143.

[12] Bao-An Li, D.H.E. Gross, V. Lips, H. Oeschler, Phys. Lett. B335 (1994) 1.

[13] S.P. Avdeyev et al., Eur. Phys. J. A3 (1998) 75.

[14] K. Kwiatkowski et al., Phys. Rev. Lett., 74 (1995) 3756.

[15] V. Lips et al., Phys. Lett. B338 (1994) 141.

[16] L. Beaulieu et al., Phys. Lett. B463 (1999) 159.

[17] T. Lefort et al., Nucl-ex/9910017.

[18] S.Y. Shmakov et al., Yad. Fiz. 58 (1995) 1735; (Phys. of Atomic Nucl. 58 (1995) 1635.

[19] G. Wang et al., Phys. Rev. C53 (1996) 1811.; G. Wang et al. Phys. Rev. C57 (1998) R2786.

[20] S.P. Avdeyev et al., Pribory i Tekhnika Eksper. 39 (1996) 7; (Instr. Exp. Techn. 39 (1996) 153).

[21] S.P. Avdeyev et al., Nucl. Instrum. Meth. A332 (1993) 149.

[22] E.R. Foxford et al., Phys. Rev. C54 (1996) 749.

[23] V.D. Toneev, K.K. Gudima, Nucl. Phys. A400 (1983) 173c.

[24] J. Bondorf et al., Phys. Rep. 257 (1995) 133; Nucl. Phys. A444 (1985) 476; A.S. Botvina, A.S. Iljinov, I.N. Mishustin, Nucl. Phys. A507 (1990) 649; A.S. Botvina et al., Phys. of Atomic Nuclei 57 (1994) 628.

[25] W.A. Friedman, Phys. Rev. C42 (1990) 667.

[26] V.D. Toneev et al., Nucl. Phys. A519 (1990) 463c.

[27] N.S. Amelin et al., Yad. Fiz. 52 (1990) 272 (Translated as Sov. Journ. of Nuclear Phys. 52 (1990) 172).

[28] K.K. Gudima et al., Yad. Fiz. 21 (1975) 602 (Translated as Sov. Journ. of Nuclear Phys. 21 (1975) 502).

[29] M. Blann, Ann. Rev. Nucl. Sci. 25 (1975) 123.

[30] C.A. Ogilvie et al., Phys. Rev. Lett. 67 (1991) 1214.

[31] H. Oeschler et al., Preprint IKDA 98/23, TU-Darmstadt.

[32] K.B. Morlet et al., Phys. Lett. B355 (1995) 52.

[33] N.T. Porile et al., Phys. Rev. C39 (1989) 1914.

[34] A.S. Botvina et al., Nucl. Phys. A584 (1995)737.

[35] S.P. Avdeyev et al., JINR Rapid Communications 2[82] (1997) 71.

[36] J.A. Hauger et al., Phys. Rev. 77 (1996) 235.

[37] A. LeFevre, M. Ploszajczak and V.D. Toneev, Phys. Rev. C60 (1999) R051602.

[38] A.S. Hirsch et al., Phys. Rev. C29 (1984) 508.

[39] P.J. Siemens, Nucl. Phys A428 (1984) 189c.

[40] M.E. Fischer, Physics 3 (1967) 255.

[41] V.A. Karnaukhov, Phys. of Atomic Nuclei 60 (1997) 1780.

[42] J. Schmelzer, G. Ropke, F.-P. Ludwig, Phys. Rev. C55 (1997) 1917.

[43] I.N. Mishustin, Nucl. Phys. A447 (1985) 67c.

[44] A. Guarnera et al., Preprint Ganil, P-95-05, 1995.

[45] J.P. Bondorf et al., Nucl. Phys. A296 (1978) 320. Nucl. Phys. A296 (1978) 320.

[46] W. Reisdorf et al., Nucl. Phys. A612(1997)493.
G.D. Kunde et al., Phys. Rev. Lett. 74 (1995) 38.

[47] J. Lauret et al., Phys. Rev. C57 (1998) R1051.

[48] D.H.E. Gross, Rep. Progr. Phys. 53 (1990) 605.

[49] W. Reisdorf, H.G. Ritter, Ann. Rev. Nucl. Part. Sci. 47(1990).

Received by Publishing Department
on June 29, 2000.